Published in final edited form as:
J Immunol. 2012 July 15; 189(2): 793–803. doi:10.4049/jimmunol.1200411.

Murine Lupus Susceptibility Locus *Sle1c2* Mediates CD4+ T cell Activation and Maps to Estrogen-Related Receptor Gamma *Esrrg*

Daniel J. Perry[*], **Yiming Yin**[*], **Tiffany Telarico**[†], **Henry V. Baker**[‡], **Igor Dozmorov**[§], **Andras Perl**[†], and **Laurence Morel**[*,1]

[*] Department of Pathology, Immunology, and Laboratory Medicine, University of Florida, Gainesville, FL 32610

[†]Departments of Medicine, Pathology, and Microbiology and Immunology, State University of New York, College of Medicine, 750 East Adams Street, Syracuse, NY 13210, USA

[‡]Department of Microbiology and Molecular Genetics, University of Florida, Gainesville, FL 32610

[§]Oklahoma Medical Research Foundation, Oklahoma City, OK 73104

Abstract

Sle1c is a sublocus of the NZM2410-derived *Sle1* major lupus susceptibility locus. We have previously shown that *Sle1c* contributes to lupus pathogenesis by conferring increased CD4$^+$ T cell activation and increased susceptibility to chronic graft-versus-host disease (cGVHD), which mapped to the centromeric portion of the locus. In this study, we have refined the centromeric sublocus to a 675Kb interval, termed *Sle1c2*. Mice from recombinant congenic strains expressing *Sle1c2* exhibited increased CD4$^+$ T cell intrinsic activation and cGVHD susceptibility, similar to mice with the parental *Sle1c*. In addition, B6.*Sle1c2* mice displayed a robust expansion of IFNγ expressing T cells. NZB complementation studies showed that *Sle1c2* expression exacerbated B cell activation, autoAb production, and renal pathology, verifying that *Sle1c2* contributes to lupus pathogenesis. The *Sle1c2* interval contains two genes, only one of which, *Esrrg*, is expressed in T cells. B6.*Sle1c2* CD4$^+$ T cells expressed less *Esrrg* than B6 CD4$^+$ T cells, and *Esrrg* expression was negatively correlated to CD4$^+$ T cell activation. *Esrrg* encodes for an orphan nuclear receptor that regulates oxidative metabolism and mitochondrial functions. In accordance with a reduced *Esrrg* expression, B6.*Sle1c2* CD4$^+$ T cells present reduced mitochondrial mass and altered mitochondrial functions, as well as altered metabolic pathway utilization when compared to B6. Taken together, we propose *Esrrg* as a novel lupus susceptibility gene regulating CD4$^+$ T cell function through their mitochondrial metabolism.

Introduction

The murine NZM2410 strain spontaneously develops an autoimmune disease that mimics systemic lupus erythematosus (SLE), including the presence of anti-nuclear autoAb (ANA), immune activation, and immune-complex induced glomerulonephritis (GN). Derived from the classic (NZB × NZW)F1 (NZB/W F1) lupus model, it has an advantage over its parental

Address correspondence and reprint requests to Dr. Laurence Morel, Department of Pathology, Immunology, and Laboratory Medicine, University of Florida, Box 100275, Gainesville, FL 32610. morel@ufl.edu.

[1]Supported by NIH grants R01 AI045050 to LM and AI072648 to AP.

Public databases accession numbers The microarray data sets accession number in Geo (http://www.ncbi.nlm.nih.gov/geo/) is GSE31702.

strains in that it is homozygous, making it an ideal model to identify novel genetic determinants of lupus (1). Linkage analysis of NZM2410 to GN identified the major lupus susceptibility locus, *Sle1*, as an NZW-derived interval on telomeric chromosome 1 (2). This region overlaps with syntenic human SLE QTLs, 1q22–23 and 1q41–42, suggesting that similar genetic factors may mediate pathogenesis in both species (3). Subsequent studies using congenic mice demonstrated distinct functional requirements that *Sle1* imparted in the induction of murine lupus. Specifically, B6.*Sle1* mice display B and T cell intrinsic loss of tolerance to chromatin (4–6). Furthermore, complementation analyses with the other NZM2410-derived SLE susceptibility loci (7) and with the NZW genome (8) demonstrated that *Sle1* expression was necessary for disease to develop in this model. Still, the identification of the underlying genetic determinants of SLE pathogenesis in this 62 Mb region, which contains an estimated 350 genes, remained a daunting task.

Three *Sle1* subloci, *Sle1a, Sle1b*, and S*le1c*, contribute to the production anti-chromatin autoAbs, revealing the complexity of this locus (9). Further phenotypic characterization of these subloci revealed increased activation of $CD4^+$ T cells by *Sle1a* and *Sle1c* and defective B cells tolerance by *Sle1b* (9–11). Using congenic recombinants, *Sle1c* was determined to correspond to at least two subloci, *Sle1c1* and *Sle1c2* (12). Complement receptor 2 (*Cr2*) was identified as a candidate gene for *Sle1c* (3), and subsequently found to co-segregate with the telomeric *Sle1c1* (12). Ensuing human association studies validated these findings by identifying a haplotype that alters *CR2* splicing that was associated with SLE (13, 14). Additionally, *Sle1b* has been attributed to polymorphisms in the SLAM gene cluster, with direct evidence for one SLAM family member *Slamf6* (11, 15, 16). More recently, evidence has shown that expression of *Slamf1, Slamf2* and *Slamf4*, other members of the SLAM family located within *Sle1b*, are also involved in controlling ANA production (17, 18). Finally, *Sle1a1* corresponds to a novel splice isoform of *Pbx1*, which is found more frequently in SLE patients than in healthy controls (19). Thus, a variety of novel lupus susceptibility genes have been identified so far in the *Sle1* locus affecting both B and T cell functions.

We have previously reported that *Sle1c2* is associated with increased activation and proliferation of $CD4^+$ T cells (12). In the current study, we mapped *Sle1c2* to estrogen-related receptor gamma (*Esrrg*), which encodes for the orphan nuclear receptor, ERRγ. The expression of this gene, which regulates oxidative metabolism (20), has not been previously been reported in T cells. We showed that the NZW allele is associated with a reduced *Esrrg* expression in $CD4^+$ T cells, which strongly correlates with increased cell activation, and the expansion of IFNγ secreting T cells. In addition, B6.*Sle1c2* $CD4^+$ T cells showed a reduced mitochondrial mass and hyperpolarization consistent with their reduced *Esrrg* expression. Finally, we demonstrated that *Sle1c2* contributes to lupus phenotypes in two disease models. These results suggest that *Esrrg* is a novel lupus susceptibility gene that regulates $CD4^+$ T cell function and activation through their mitochondrial metabolism.

Materials and Methods

Mice

B6.*Sle1c* mice that contain a NZW-derived interval at the telomeric end of chromosome 1 have been described previously (9). The loci previously referred to as *Sle1c.Cr2*^{w}*-1* on the telomeric end and *Sle1c.Cr2*^{b}*-1* on the centromeric end (12) have been renamed *Sle1c1* and *Sle1c2* respectively to be more consistent with the terminology of the other loci. To generate additional recombinant subcongenic strains, (B6 × B6.*Sle1c*)F1 × B6 backcross progeny were genotyped for recombinations in the *Sle1c* interval with microsatellites that are polymorphic between NZW and B6. Recombinants were bred to B6 and the progeny of this expansion backcross were then bred to homozygosity. To fine-map the ends of the

recombinant congenic intervals, single nucleotide polymorphisms (SNPs) that are polymorphic for B6 and NZW were selected from the Mouse Phenome Database (http://phenome.jax.org/SNP), and alleles were determined by sequencing. C57BL/6 (B6), B6.Cg-Tg(TcraTcrb)425Cbn/J (B6.OTII), B6(C)-H2-Ab1^{bm12}/KhEgJ (B6.bm12), B6.Cg-Igh^{a}Thy1^{a}Gpi1^{a}/J (B6.*Thy1^{a}*), B6.129P2-*Tcrb^{tm1Mom}Tcrd^{tm1Mom}*/J (B6.*Tcrbd$^{-/-}$*), and NZB mice were purchased from the Jackson Laboratory. B6.FoxP3-eGFP mice (21) were a kind gift from Dr. Vijay Kuchroo (Harvard Medical School). All mice were bred and maintained at the University of Florida in specific pathogen-free conditions and experiments were performed using age and sex-matched cohorts at the ages indicated in the text. All experiments were conducted according to protocols approved by the University of Florida Institutional Animal Care and Use Committee.

Cell isolation and culture

Single cell suspensions were prepared from spleen and red blood cells were lysed. Cells were then washed in ice cold 5% FCS in PBS and passed through 30μm nylon mesh to remove debris. Splenocyte suspensions were enriched for CD4^{+} T cells by negative selection with magnetic beads (Miltenyi). RPMI supplemented with 10% FCS, HEPES, 2-Mercaptoethanol, and penicillin-streptomycin was used as culture medium. Cells were stimulated either with plate-bound 5μl/ml anti-CD3e (145-2C11) and 2.5μl/ml anti-CD28 (37.51) (BD Biosciences), or with 0.5μg/ml PMA and 1μM ionomycin (Sigma). For Ag-specific proliferation assays, irradiated (2000 Rad) B6 splenocytes were pulsed for 2 h at 37°C with either OVA$_{323–339}$ or histone H4$_{76–90}$ at the indicated concentrations. The Ag-loaded splenocytes were then co-cultured 1:1 with CD4^{+} T cells from B6.OTII or B6.*Sle1c2*.OTII mice in triplicate. ^{3}H-thymidine was added at 1 μCi/ 200μl for the last 18 h of 72 h cultures to measure proliferation. Cells were then harvested onto glass filter paper to measure thymidine incorporation. For T$_{H}$17 polarization, CD4^{+} T cells were cultured with anti-CD3e and anti-CD28, 2.5 ng/ml TGF-β (Peprotech), and 25 ng/ml IL-6 (Peprotech) for 48 h. For CD4^{+} FoxP3^{+} regulatory T cell (Treg) induction, FACS-sorted CD4^{+}GFP$^{−}$ T cells from B6.FoxP3-eGFP or B6.*Sle1c2*.FoxP3-eGFP mice were cultured with anti-CD3e and anti-CD28, and 2.5 ng/ml TGF-β with or without 10 nM all-trans-retinoic acid (atRA, Sigma).

Flow cytometry

Cell suspensions were blocked with 10% normal rabbit serum and anti-CD16/32 (2.4G2) in staining buffer (5% FCS, 0.05% sodium azide in PBS) and incubated on ice for 30 min. Biotinylated or fluorophore-conjugated Abs specific for CD3 Molecular Complex (17A2), CD4 (RM4-5), CD8a (53–6.7), CD44 (IM7), CD62L (MEL-14), CD25 (7D4), CD69 (H1.2F3), CD90.1 (OX-7), CD90.2 (53–2.1), B220 (RA3-6B2), CD19 (1D3), IgM (II/41), CD80 (16-10A1), CD86 (GL1), I-Ab (AF6-120.1), and isotype controls were used in predetermined amounts. SA-PerCP-Cy5.5 (BD Biosciences) was used to detect biotinylated Abs. IFNγ (XMG1.2), IL-4 (11B11), IL-17A (TC11-18H10), and FoxP3 (FJK-16s) were detected using Fixation/Permeabilization kits (eBiosciences) according to manufacturer's protocol. When cytokine profiles were analyzed, cells were treated with leukocyte activation cocktail (BD Biosciences) prior to staining. All Abs were from BD Biosciences except for anti-FoxP3, which was from eBiosciences. Analysis was performed on a FACSCalibur cytometer (BD Biosciences) with at least 50,000 events per sample collected, and lymphocyte populations were gated based on forward and side scatter characteristics.

For metabolic labeling, splenocytes derived from 2–3 month old B6, B6.*Thy1^{a}*, and B6.*Sle1c2* mice were stained in RPMI 1640 medium at a density of 1 × 10^{6} cells/ ml with cell-permeable metabolic dyes at 37°C for 30–120 min, followed by surface staining with PE Cy7 conjugated CD3 (17A2), PerCP conjugated CD4 (GK1.5), APC Cy7 conjugated

CD8a (53–6.7), PE conjugated CD11b (M1/70), APC conjugated CD11c (N418), and Alexa Fluor 700 conjugated CD19 (6D5) Abs for 30 min at 4°C. All Abs for this experiment were obtained from Biolegend. Metabolic indicators were used for measurement of NO, mitochondrial transmembrane potential, mitochondrial mass, Ca^{2+} stores, superoxide production, apoptosis, and necrosis (27,28). Diaminorhodamine-4M (DAR-4M) was used to evaluate peroxynitrite production, a byproduct of increased NO production. Mitochondrial transmembrane potential was measured using potentiometric indicator tetramethylrhodamine methyl ester (TMRM). Mitochondrial mass was measured by fluorescence of MitoTracker Green-FM (MTG). Calcium stores were measured by fluorescence of Fluo-3 AM (1 μM). Hydroethidine (HE), dihydrorhodamine 123 (DHR) and 2′,7′-dichlorofluorescin (DCF) were used as an indicator for superoxide production. Apoptosis and necrosis were evaluated by co-staining with FITC conjugated Annexin V and propidium iodide (PI). TMRM, MTG, HE, Fluo-3M and PI were obtained from Invitrogen-Molecular Probes, DAR-4M from Calbiochem, and FITC conjugated Annexin V was from BD Biosciences. The metabolic profiling was evaluated on a LSR-II flow cytometer (BD Biosciences), with 50,000 events per sample collected. Data was analyzed using Flow Jo cytometry analysis software (TreeStar, Ashland, OR). MFI values of B6.*Sle1c2* mice were normalized to the means obtained for B6 mice studied in parallel and set at 1.0.

Gene expression analyses

Total RNA was isolated using RNeasy mini kits, Qiashredders, and RNase-free DNase sets (Qiagen). cDNA was then synthesized using the ImProm-II Reverse Transcription System (Promega). Primers for ERRγ target genes (Supplemental Table 1) were designed with the Primer3 software (http://frodo.wi.mit.edu/primer3/) and used in Sybr® Green (Applied Biosystems) based qRT-PCR. Taqman Gene Expression Assays (Applied Biosystems) were used to measure *Esrrg* (Mm00516269_mH, spans exons 3 and 4 of transcript 1) and *Gapdh* control expression. Relative quantity of gene expression was calculated using the comparative C_T method ($RQ=2^{-\Delta\Delta Ct}$) normalized to the average ΔC_T of the B6 samples. Global gene expression was compared between negatively-bead selected $CD4^+$ T cells from 6 month old B6 and B6.*Sle1c2* mice (n=5 per strain). Their cDNA was synthesized, fragmented, and biotin-labeled using the Ovation Biotin RNA Amplification and Labeling System (NuGEN Technologies), then hybridized to Affymetrix Mouse Genome 430 2.0 arrays. Data analysis was based on the use of “internal standards” and generalization of the “Error Model” (22) as presented elsewhere (23).

ELISA

Anti-dsDNA and anti-chromatin IgG were measured by ELISAs as previously described (4). Sera were tested in duplicate in a 1:100 dilution. Relative units were standardized using serial dilutions of a positive serum from a B6.*Sle1.Sle2.Sle3* (BcN/LmoJ) mouse, arbitrarily setting the 1:100 dilution reactivity to 100 units.

Western blots

Cell lysates prepared from splenic $CD4^+$ T cells purified by negative selection were probed with rabbit polyclonal ERRγ Ab (Z-21, Santa Cruz Biotechnology) and revealed with horseradish peroxidase-conjugated anti-rabbit IgG (Sigma Aldrich). Horseradish peroxidase-conjugated anti-GAPDH Ab (Sigma Aldrich) was used as control. The membranes were developed by enhanced Supersignal West Pico Chemiluminescent substrate (Thermo Scientific, Rockford, IL). The bands were quantified using Alphaview software (Alpha Innotech).

For VDAC (voltage-dependent anion channel) expression, protein lysates were prepared from splenocytes and negatively-isolated T cells (Dynal mouse T cell isolation kit,

Invitrogen) through lysis in radio-immunoprecipitation assay buffer (150 mM NaCl, 2% NP-40, 0.5% sodium deoxycholate, 0.1% SDS, 50 mM Tris pH 8.0, 1 mM PMSF, 1 μg/ml aproptinin, 1 μg/ml pepstatin, 1 g/ml leupeptin, 1 mM NaF, 1 mM sodium orthovanadate, 0.1 mM sodium molybdate, 10 mM sodium pyrophosphate) at a density of 4×10^7 cells/ml on ice, followed by addition of equal volumes of Laemmli buffer and were heated to 95°C for 5 min prior to separation on SDS-PAGE gels and transfer to 0.45 μm nitrocellulose membranes. VDAC / porin was detected with rabbit polyclonal Ab (Abcam #ab34726), and β-actin was detected with mouse monoclonal Ab (Millipore #MAB1501R). Western blots were imaged using a Kodak Image Station 440CF and quantified by automated densitometry using Kodak1D software (Eastman Kodak, Rochester NY).

Mixed bone marrow chimera

Chimeras were prepared as previously described (5). Briefly, 4–5 month old B6.*Tcrbd*$^{-/-}$ recipients were lethally irradiated with two doses of 525 Rad 4–6 h apart the day before reconstitution. Bone marrow (BM) cell suspensions from B6.*Thy1*^{a} and B6.*Sle1c2* were mixed 1:1 after depleting T cells using anti-CD5 magnetic beads (Miltenyi). Recipients received 10^7 BM cells from sex-matched donors by i.v. injections and grafts were allowed to reconstitute for 8 weeks.

Chronic Graft versus host disease (cGVHD)

cGVHD was induced as previously described (24). Briefly, B6 and B6.*Sle1c2* hosts received 8×10^7 B6.bm12 splenocytes via i.p. injections. Sera were collected weekly after induction and screened for anti-dsDNA and anti-chromatin IgG. Hosts were sacrificed 3 weeks after transfer, kidneys were prepared for histology, and splenocytes were analyzed by flow cytometry. The presence of immune complexes in the kidneys was evaluated on frozen tissue sections stained with FITC-conjugated anti-C3 (Cappel) and anti-IgG H+L chains (Jackson Immunoresearch). Staining intensity was evaluated in a blind manner on a semi-quantitative 0–3 scale and averaged on at least 10 glomeruli per section. Two separate sets of cGVHD induction were performed with at least five mice per strain, yielding similar results.

Experimental autoimmune encephalomyelitis (EAE)

EAE was induced in 4-month-old male B6 or B6.*Sle1c2* mice. On d 0, mice received an emulsion of 50μg myelin oligodendrocyte glycoprotein (MOG) peptide sequence 35–55 ($MOG_{35–55}$) and 500 μg of *Mycobacterium tuberculosis* (Difco) in incomplete Freund's adjuvant (Sigma) via subcutaneous injections at the base of the tail. Additionally, 500 ng of pertussis toxin (List Biologicals) was administered i.p. on d 0 and 2. Daily clinical scores were assessed by the following criteria: 0, no disease, 1, flaccid tail, 2, hind limb paraparesis, 3, hind limb paralysis, 4, quadriplegia. Mice were euthanized at a score of 4, or after a 40 d after induction.

Statistical analysis

Statistical analyses were performed using the GraphPad Prism 5 software. Unless indicated, graphs show mean and SEM for each group. For comparisons between two groups, two-tailed Mann-Whitney were used when $n \geq 5$ and Student's *t*-tests were used either when $n < 5$, or when data sets passed D'Agostino and Pearson omnibus normality tests as indicated. ANOVA with Dunn's post-test and 2-way ANOVA with Bonferroni post-test corrections were used for multiple comparisons as appropriate. Each *in vitro* experiment was performed at least twice.

Results

Increased CD4+ T cell activation maps to the centromeric end of Sle1c

In order to narrow down the number of candidate genes responsible for the increased $CD4^+$ T cell activation displayed by *Sle1c* congenic mice, six subcongenic strains were generated in which recombinant screening was targeted to the centromeric end of the interval (Fig. 1A). Phenotypic screening showed that two strains, REC2b and REC5, displayed increased spleen weight and CD4:CD8 T cell ratio in aged mice as compared to B6 (Fig. 2A). Additionally, these two strains displayed increased $CD4^+$ T cell activation with a significantly higher percentage of $CD69^+$ T cells and of $CD44^{hi}$ $CD62L^-$ T effector memory cells (Tem). Since the strain with the shortest interval necessary for increased activation is the REC5 subcongenic, and REC1, 2, 3, and 8 were B6-like, *Sle1c2* was then defined as the 675Kb region between SNPs rs30920616 and rs32528185 (Fig. 1A and B). Except where noted, the REC5 strain was used as B6.*Sle1c2* for the remainder of this study.

As opposed to the splenomegaly phenotype, which is age-dependent, $CD4^+$ increased activation was detectable as early as 2–3 months of age (Supplemental Fig. 1A), suggesting that it is a primary consequence of *Sle1c2* expression. Importantly, as previously shown for the entire *Sle1c* interval (12), a mixed BM chimera experiment showed that increased $CD4^+$ T cell activation was intrinsic to *Sle1c2*-expressing T cells (Supplemental Fig. 1B). Since we have previously reported an increased proliferation of B6.*Sle1c* $CD4^+$ T cells (12), we screened the congenic recombinants to discern whether this phenotype also mapped to the refined *Sle1c2* locus. To assess whether the increased proliferation was antigen-specific, B6.*Sle1c2*.OTII double-congenic mice were generated for comparison to B6.OTII mice, which carry a transgenic TCR that is specific for the OVA323-339 ovalbumin peptide. Increased proliferation was observed with Ag-specific OVA (Fig. 2B), polyclonal TCR (Fig. 2C) and PMA/ionomycin (Fig. 2D) stimulation of B6.*Sle1c2*.OTII as compared to B6.OTII T cells. This increased activation and proliferation resulted in an expansion of the $CD4^+$ T cell compartment in older mice, specifically Tem to the expense of naïve $CD4^+$ T cells (Fig. 2E). Age-dependent expansion of the B and $CD8^+$ T cell compartments were also observed in B6.*Sle1c2* mice (Fig 2F). However, surface marker analysis found no evidence of increased activation in these cells (not shown). Taken together, these results mapped the $CD4^+$ T cell activation phenotype observed in *Sle1c* mice to the 675 Kb *Sle1c2* interval. This drastically reduced the set of candidate genes from 48 to 2, namely *Esrrg*, encoding Estrogen-related receptor gamma, and *Ush2a*, encoding for Usher syndrome 2A homolog (Fig. 1B).

B6.Sle1c2 CD4+ T cells exhibit a marked TH1 skewing

A gene expression and pathway analysis of $CD4^+$ splenocytes revealed that a large number of genes related to IFNγ expression were upregulated in B6.*Sle1c2* mice, suggesting a TH1 skewing (Supplemental Fig. 2A, 2B). Intracellular staining confirmed that a larger percentage of *Sle1c2* $CD4^+$ splenocytes expressed IFNγ as compared to B6 (Fig. 3A). Importantly, $CD4^+$ T cells from the parental B6.*Sle1c* strain showed a similar percentage of $IFN\gamma^+$ as the B6.*Sle1c2* subcongenic strain. No difference was observed for IL-4 production (data not shown).

The microarray analysis also revealed that several genes involved in TH17/Treg homeostasis were upregulated in B6.*Sle1c2* $CD4^+$ T cells (Supplemental Fig. 2C). These included *FoxP3*, *Il2ra*, and *IL10* for Treg cells, and *Irf4*, *Rora*, *Il17a*, *IL21*, and *Il22*, for TH17 cells. Additionally, the *Ahr* and *Hif1a* pathways, which have been implicated in TH17/Treg homeostasis (25–27) were also upregulated (Supplemental Fig. 2B–C). Given this altered gene expression profile, we examined whether *Sle1c2* expression augmented Treg and TH17

differentiation. Using FoxP3-eGFP reporter mice, we showed that TGFβ with or without atRA equally induced FoxP3 expression in B6 and B6.*Sle1c2* $CD4^+$ GFP^- T cells (Supplemental Fig. 1C). Moreover, contrary to our previous reports that described a decrease in the percentage of Treg defined as $CD4^+$ $CD62L^+$ $CD25^+$ (10, 12), the size of the $CD4^+$ $FoxP3^+$ Treg compartment was similar between B6 and B6.*Sle1c2* mice, with an expansion of $FoxP3^+$ Treg in older B6.*Sle1c2* mice (Supplemental Fig. 1D). Interestingly, *in vitro* Treg polarization produced significantly more $FoxP3^+$ $IFN\gamma^+$ cells in B6.*Sle1c2* mice at 8–10 month old, but not 1–3 month old (Fig. 3B and D). This not only confirms the strong TH1 skewing associated with *Sle1c2*, but also suggests that B6.*Sle1c2* mice may accumulate Tregs corresponding to a plastic population of $IFN\gamma^+$ adaptive Tregs that have been linked to autoimmunity (28).

TH17 *in vitro* polarization did not reveal differences in IL-17 production between the two strains (Fig. 3C and D). However, as with Treg polarization, IFNγ production was increased in the B6.*Sle1c2* TH17 polarized $CD4^+$ T cells (Fig. 3C and D), highlighting again the TH1 skewing induced by *Sle1c2* expression. Finally, EAE was used as a model to test for differences in TH17/Treg homeostasis *in vivo*, and no differences were observed in day of onset or severity between the two strains (Supplemental Fig. 1E). Hence, while the global gene expression analysis predicted increased commitment to TH1, Treg, and TH17 lineages, cellular assays only revealed a strong TH1 skewing.

Sle1c2 exacerbates lupus in the induced cGVHD model and via epistatic interactions with the NZB genome

To determine whether the $CD4^+$ T cell phenotypes that segregate with *Sle1c2* are relevant to lupus pathogenesis, we used the cGVHD-induced lupus model (29). Preliminary results mapped an increased cGVHD susceptibility to the centromeric portion of *Sle1c* that includes *Sle1c2* (12). Here we showed that $CD4^+$ T cells were significantly more activated in B6.*Sle1c2* recipients of B6.bm12 splenocytes as compared to B6 recipients (Fig. 4A). In addition, B6.*Sle1c2* $CD11c^+$ dendritic cells and B cells displayed altered activation (Fig. 4B and C) that was concurrent with increased serum autoAb production (Fig. 4D). Finally, the kidneys of cGVHD-induced B6.*Sle1c2* mice showed an increased deposition of IgG2a immune complexes as compared to B6 (Fig. 4E). These results demonstrate that the activated phenotype of *Sle1c2* $CD4^+$ T cells contributes to induced humoral autoimmunity.

We have previously shown that *Sle1c* expression increases lupus phenotypes presented by (NZB × B6)F1 hybrids (30). Using the same model, we compared the phenotypes of (NZB × B6)F1 and (NZB × B6.*Sle1c2*)F1 mice, in which the NZB hemi-genome interacts with either the B6 or the NZW *Sle1c2* alleles, respectively. Importantly, the NZB and NZW share the same haplotype at the chromosome 1: 189.80–190.050 Mb interval that includes the *Sle1c2* portion of *Esrrg*, as determined for all 228 published SNPs that are polymorphic between B6 and NZW, with an NZB allele known or imputed with confidence ≥ 0.9 (data not shown). Therefore, the *Sle1c2* locus is predicted to be homozygous for the NZB/NZW allele in (NZB × B6.*Sle1c2*)F1 mice, and heterozygous in (NZB × B6)F1 mice. This is relevant because the *Sle1c2* $CD4^+$ T cell phenotype is recessive (data not shown). Our findings showed that in 12 month old NZB hybrids, splenomegaly, CD4:CD8 T cell ratio, percentage of Tem, and B7-2 expression on B cells were significantly increased in mice with the homozygous NZW *Sle1c2* allele (Fig. 5A). Moreover, the expression of *Sle1c2* significantly enhanced the production of anti-dsDNA IgG triggered by the NZB hemi-genome as the mice aged (Fig. 5B). Finally, IgG immune complex deposition was greatly exacerbated by *Sle1c2* (Fig. 5C–D), but did not result in clinical disease. Taken together, this data establishes that *Sle1c2* can contribute to lupus through interactions with the NZB genome.

Esrrg expression is downregulated in B6.Sle1c2 CD4$^+$ T cells

The 675Kb *Sle1c2* interval contains 2 protein-coding genes, *Esrrg* and *Ush2a* (Fig. 1B), with the latter having no detectable expression in CD4$^+$ cells (data not shown). *Esrrg* message expression was detected in CD4$^+$ splenocytes, and at a lower level in CD4$^-$ splenocytes and in thymocytes (Fig. 6A). Furthermore, *Esrrg* expression was significantly lower in the B6.*Sle1c2* CD4$^+$ as compared to B6 CD4$^+$ fraction (40.6 ± 11.4% less). No difference between strains was observed in CD4$^-$ splenocytes. *Esrrg* expression in CD4$^+$ T cells is low compared to liver, heart, brain and kidney, highly metabolic tissues in which *Esrrg* expression has been reported (31–33), going from about 4 times lower than in liver to about 50 times lower than in kidney (Supplemental Fig. 3A). In our microarray analysis, five probes were located within the *Esrrg* locus (with only one actually probed the ERRγ coding sequence). However, the signal for all 5 probes was below the detectable threshold. CD4$^+$ T cell ERRγ protein expression was detected in CD4$^+$ T cells (Fig. 6B). We were not able, however, to show a difference between B6.*Sle1c2* and *B6. Esrrg* overexpression in cell lines showed that messages and protein levels were not tightly correlated, suggesting an important post-transcriptional regulation (data not shown). Regardless of age or strain, *Esrrg* message expression in splenic CD4$^+$ T cells showed a strong negative correlation with both CD69$^+$ and Tem percentages (Fig. 6C), suggesting that *Esrrg* negatively regulates CD4$^+$ T cell activation.

Esrrg expression was compared between B6.*Sle1c2* and B6 adult brain, heart, kidney, and liver. *Esrrg* expression was significantly decreased in B6.*Sle1c2* brain, and a trend for decreased expression was observed in kidney and liver (Supplemental Fig. 3B). Interestingly, an opposite trend was observed in heart. *Esrrg*-deficient mice die postnatally due to a defective switch from glycolytic to oxidative metabolism (34). Consistent with this result and a reduced *Essrg* expression in *B6.Sle2c2* mice, we have observed a high mortality in B6.*Sle1c2* neonates (69% total litter loss, corresponding to 34 litters lost out of 49 born) as compared to B6 (18% litter loss corresponding to 13 out 71 born during the same period of time and in the same room). It is possible that in response to reduced *Esrrg* expression, a compensatory mechanism may increase *Esrrg* expression in the myocardium of a percentage of B6.*Sle1c2* neonates, resulting in their survival.

To determine if decreased *Esrrg* expression in CD4$^+$ T cells had transcriptional consequences on its putative targets, we selected 12 genes (Supplemental Table I) that were differentially expressed by B6.*Sle1c2* CD4$^+$ T cells in the microarray analysis and that were also known to have ERRγ bound to their promoters by chip-on-chip analyses (34, 35). The expression of five of these genes, transcriptional regulators c-myc binding protein (*Mycbp*) and retinoic acid receptor alpha (*Rara*), a subunit of electron transport complex I (*Ndusf1*), a mitochondrial protein modifier (*Ppif*), and a mitochondrial oxidoreductase (*Rtn4ip1*), was significantly decreased in *Sle1c2* CD4$^+$ T cells (Supplemental Fig. 3C). This data suggest that the decreased *Esrrg* expression induced by *Sle1c2* affects *Esrrg* target gene expression.

Since *Esrrg* is known to regulate glycolytic and oxidative metabolic programs (34), we analyzed the expression of several genes involved in these pathways by quantitative PCR. *Hif1*α and *Slc16a3*, encoding for monocarboxylic acid transporter 4 (MCT4), which are both mediators of glycolysis (27), were expressed at a higher level in B6.*Sle1c2* CD4$^+$ T cells (Fig. 6D). In addition to glycolysis, a microarray pathway analysis revealed an influence of *Sle1c2* in several other metabolic pathways, including glutaminolysis, glycogenesis, and fatty acid oxidation (Fig. 6E). Furthermore, genes regulating electron transport chain were also differentially regulated, indicating altered mitochondrial function. Finally, out of the 7 metabolic genes that were analyzed in both the Esrrg$^{-/-}$ heart (34) and the *Sle1c2* CD4$^+$ T cells in this study, five of them (*Eno2*, *Gsk3*, *Cox6a2*, *Ndufa10* and *Ndufs1*) showed an expression change in the same direction. Overall, these data provide

evidence that *Sle1c2* results in an altered metabolic profile in $CD4^+$ T cells, due to decreased *Esrrg* expression.

B6.Sle1c2 $CD4^+$ T cells exhibit mitochondrial dysfunction

Esrrg expression has been reported to directly correlate with mitochondrial biogenesis and functions (33). Accordingly, a decreased *Esrrg* expression is predicted to reduce mitochondrial mass and functions in *Sle1c2* $CD4^+$ T cells. This was indeed verified in the spleen of 2–3 month old mice, in which the difference in T cell activation is still minimal, and therefore not likely to induce secondary metabolic changes. The mitochondrial membrane potential and mass were significantly decreased in *Sle1c2* $CD4^+$ T cells as compared to B6 (Fig. 7A and B), and this was associated with decreased Ca^{2+} and NO levels (Fig. 7D and E). In turn, the production of reactive oxygen intermediates (ROI), as measured by HE fluorescence, was increased in *Sle1c2* $CD4^+$ T cells. However, no difference in ROI was found between the two strains when measured with the DCF or DHR dyes (data not shown). These findings are suggestive of mitochondrial dysfunction, characterized by an inability to maintain transmembrane potential while leaking ROI. Consistent with impaired mitochondrial functions, a significant increase of necrosis was observed in *Sle1c2* splenocytes (Fig. 7F). This corresponds to a predisposition to pro-inflammatory death by necrosis that has been previously reported in lupus T cells (36).

Interestingly, VDAC levels were significantly increased in *Sle1c2* $CD4^+$ T cells (Fig. 7G), which may correspond to a compensatory mechanism to maintain mitochondrial membrane potential in spite of reduced *Esrrg* expression. A reduced mitochondrial mass was not observed in other *Sle1c2* immune cell populations, except $CD11c^+$ cells (Table 1). This may be related to the fact that *Esrrg* expression is very low in $CD4^-$ splenocytes (Fig. 6A), therefore not affecting mitochondria in these cell types. Other parameters showed significant differences between the two strains in non-$CD4^+$ cell types, such as NO levels which were significantly reduced in $CD8^+$ T cells, B cells, $CD11b^+$ and $CD11c^+$ splenocytes (Table 1), indicating that the metabolic consequences of *Esrrg* deficiency may not be confined to T cells.

Discussion

Within the major NZM2410-lupus susceptibility *Sle1* locus, increased $CD4^+$ T cell activation mapped to both *Sle1a* and *Sle1c* (10), with each of these loci corresponding to two subloci (12, 37). The current study focused on the functional characterization and mapping of the $CD4^+$ T cell phenotypes associated with *Sle1c*. Originally defined as the 7.72 Mb at the telomeric end of chromosome 1, *Sle1c* contains 48 protein-coding genes and 4 microRNAs. Previous analyses have identified *Cr2* on the temoleric end of *Sle1c* as the candidate gene associated with impaired B cell responses (3). In this study, we confirmed that centromeric *Sle1c2* enhances $CD4^+$ T cell activation, and have established that *Sle1c2* $CD4^+$ T cells are characterized by a strong TH1 skewing. In addition, we have demonstrated the contribution of *Sle1c2* to autoimmune pathology by showing that its expression enhances both induced and spontaneous lupus. Further, congenic mapping and gene expression analysis have identified *Esrrg*, one of the two genes located in the critical interval, as the candidate gene for *Sle1c2*. Finally, consistent with published works that have established that *Esrrg* is a potent regulator of mitochondrial metabolism (33), the decreased expression of *Esrrg* in *Sle1c2* $CD4^+$ T cells is associated with a decreased mitochondrial mass and with significant alterations of mitochondrial functions.

ERRγ belongs to the family of nuclear receptors, which are transcription factors whose activities are mediated by endogenous ligands and other coregulatory proteins. Several nuclear receptors have already been implicated in T cell biology, including RARα, RORγ,

PPARγ, the vitamin D and the glucocorticoid receptors, and the estrogen receptors (38–40). ERRγ, belonging to the estrogen-related receptor (ERR) family, is expressed at low levels in human spleen and thymus (41), but does not yet have an established role in T cell biology. ERRs are structurally related to estrogen receptors, but do not bind natural estrogens. In fact, ERR endogenous ligands have not been identified and they are thus referred to as orphan nuclear receptors. It has been shown, however, that ERRs are constitutively active due to properties of their ligand binding domains (42). Regardless, several synthetic compounds augment ERRγ-mediated transactivation of its target genes, demonstrating its potential as a therapeutic target (43). Interestingly, bisphenol A (BPA), an industrial component known to be an endocrine disruptor, binds to and alters the activity of ERRγ (44). BPA exposure has been linked to autoimmunity, and, relevant to this study, it has been shown to strongly downregulate IFNγ production (45). This raises the possibility that ERRγ may mediate environmental triggers of autoimmunity.

ERRs are important regulators of metabolism and energy homeostasis and *Esrrg* expression is highly restricted to metabolically active tissues (42). *Esrrg* transactivates genes involved in mitochondrial biogenesis, lipid transport and metabolism, tricarboxylic acid cycle, electron transport chain, and oxidative phosphorylation, allowing for energy production by efficient fatty acid oxidation. This vital function is demonstrated in *Esrrg* null mice, where the lack of a critical switch from glycolytic to lipid based metabolism in the myocardium results in perinatal lethality (34). Conversely, *Esrrg* overexpression in skeletal muscle resulted in increased mitochondrial biogenesis and function, as well as exercise capacity (33). Activation and proliferation by T cells is also metabolically demanding (46). However, contrary to other metabolically demanding tissues, activated T cells employ aerobic glycolysis to meet energy requirements. Known as the Warburg effect, this form of metabolism generates glucose metabolites at the expense of ATP production (47). Remarkably, when ERRγ expression is suppressed by microRNA, the Warburg effect is induced (48). The rate of glycolysis has direct consequences on $CD4^+$ T cell activation and differentiation. GLUT1 transgenic mice, which have increased glucose uptake in their T cells, show T cell activation phenotypes very similar to B6.*Sle1c2* mice, namely, age-dependent accumulation of $CD69^+$ and Tem cells, increased proliferation, and increased IFNγ production (49). Consequently, aged mice suffered from hypergammaglobulinemia and GN, exhibiting a direct connection between T cell metabolism and autoimmunity. Conversely, as recently reported in Myc-deficient mice, T cells display impaired proliferation with an altered activation phenotype when the switch to aerobic glycolysis is obstructed (50).

We hypothesize that *Sle1c2* contributes to the Warburg effect in $CD4^+$ T cells as decreased *Esrrg* expression would limit transcription of target genes that regulate oxidative lipid based metabolism, skewing toward glucose based programs. This hypothesis is supported first by the decreased expression of *Esrrg* target genes, *Ndufs1*, *Ppif*, and *Rtn4ip1* that regulate metabolism and mitochondrial function (51–53), and second by the decreased mitochondrial biogenesis and functions in *Sle1c2* $CD4^+$ T cells. Recently, Rathmell et al. reported that ERRα functions as a regulator of T cell metabolism (54). This isoform, encoded by a separate gene, *Esrra*, binds to the same DNA consensus sequence as ERRγ, and shares the same general function as a metabolic regulator. However, contrary to the increased T cell activation observed in B6.*Sle1c2* mice, which have reduced *Esrrg* expression in $CD4^+$ T cells, *Esrra*$^{-/-}$ mice lacked an expansion of Tem as they aged. Interestingly, *Esrra*$^{-/-}$ $CD4^+$ T cells were not defective in their proliferative and glycolytic capacities in response to TCR activation whereas wild-type T cells in which ERRα was acutely inhibited were deficient in these capacities. This suggested that a developmental compensatory mechanism was offsetting the effect of *Esrra* deficiency, and indeed the authors observed alterations in mTOR and AMPK pathways. At this point it is not clear why chronic ERRγ deficiency

leads to increased activation, while ERRα deficiency results in a more naïve phenotype. It is conceivable that these two isoforms utilize different cofactors to dictate their function. Overall these findings validate our observations that deficiencies in ERRγ cause globally augmented metabolism in $CD4^+$ T cells and results in altered T cell function.

Dysregulated T cells are a major contributor to SLE pathogenesis, and targeting them is an important focus for therapeutic intervention (55). Mitochondrial dysfunctions have specifically been identified as a characteristic of human lupus T cells, which may offer additional therapeutic targets (56). Recent studies have highlighted the regulation of metabolism as an important checkpoint of T cell activation and effector functions. Our study associates, for the first time, a gene known as a major regulator of metabolism, mitochondrial dysfunctions, and $CD4^+$ T cell activation TH1 polarization in a lupus model. A better understanding of the role of ERRγ in $CD4^+$ T cells will provide a better understanding of how metabolism regulates immune functions in the context of autoimmunity.

Supplementary Material

Refer to Web version on PubMed Central for supplementary material.

Acknowledgments

We thank Drs. Eric Sobel, Clayton Matthews, Alberto Riva and Margaret Wallace for valuable discussions, Leilani Zeumer and Xuekun Su for excellent technical help, and Celia Lopez for microarray processing.

Abbreviations

SLE	systemic lupus erythematosus
ANA	anti-nuclear autoAb
GN	glomerulonephritis
NZB/W F1	(NZB × NZW) F1
SNP	single nucleotide polymorphism
atRA	all-*trans* retinoic acid
B6	C57Bl/6J
B6.OTII	B6.Cg-Tg(TcraTcrb)425Cbn/J
B6.bm12	B6(C)-H2-Ab1^{bm12}/KhEgJ
B6.*Thy1*^{a}	B6.Cg-Igh^{a}Thy1^{a}Gpi1^{a}/J
B6.*Tcrbd*$^{-/-}$	B6.129P2-*Tcrb*^{tm1Mom} *Tcrd*^{tm1Mom}/J
T_{reg}	regulatory T cells
BM	bone marrow
Tem	T effector memory cells
VDAC	voltage-dependent anion channel
DAR-4M	Diaminorhodamine-4M
MTG	MitoTracker Green
HE	Hydroethidine

DIP	Deletion/Insertion polymorphism
ERR	estrogen – related receptor
BPA	bisphenol A

References

1. Perry D, Sang A, Yin Y, Zheng YY, Morel L. Murine models of systemic lupus erythematosus. J. Biomed. Biotechnol. 2011; 2011:271694. [PubMed: 21403825]
2. Morel L, Rudofsky UH, Longmate JA, Schiffenbauer J, Wakeland EK. Polygenic control of susceptibility to murine systemic lupus erythematosus. Immunity. 1994; 1:219–229. [PubMed: 7889410]
3. Boackle SA, Holers VM, Chen XJ, Szakonyi G, Karp DR, Wakeland EK, Morel L. Cr2, a candidate gene in the murine Sle1c lupus susceptibility locus, encodes a dysfunctional protein. Immunity. 2001; 15:775–785. [PubMed: 11728339]
4. Mohan C, Alas E, Morel L, Yang P, Wakeland EK. Genetic dissection of SLE pathogenesis - Sle1 on murine chromosome 1 leads to a selective loss of tolerance to H2A/H2B/DNA subnucleosomes. J. Clin. Invest. 1998; 101:1362–1372. [PubMed: 9502778]
5. Sobel ES, Mohan C, Morel L, Schiffenbauer J, Wakeland EK. Genetic dissection of SLE pathogenesis: Adoptive transfer of Sle1 mediates the loss of tolerance by bone marrow-derived B cells. J. Immunol. 1999; 162:2415–2421. [PubMed: 9973523]
6. Sobel ES, Satoh M, Chen WF, Wakeland EK, Morel L. The major murine systemic lupus erythematosus susceptibility locus Sle1 results in abnormal functions of both B and T cells. J. Immunol. 2002; 169:2694–2700. [PubMed: 12193743]
7. Morel L, Croker BP, Blenman KR, Mohan C, Huang G, Gilkeson G, Wakeland EK. Genetic reconstitution of systemic lupus erythematosus immunopathology with polycongenic murine strains. Proc. Natl. Acad. Sci. U.S.A. 2000; 97:6670–6675. [PubMed: 10841565]
8. Morel L, Tian XH, Croker BP, Wakeland EK. Epistatic modifiers of autoimmunity in a murine model of lupus nephritis. Immunity. 1999; 11:131–139. [PubMed: 10485648]
9. Morel L, Blenman KR, Croker BP, Wakeland EK. The major murine systemic lupus erythematosus susceptibility locus, Sle1, is a cluster of functionally related genes. Proc. Natl. Acad. Sci. U.S.A. 2001; 98:1787–1792. [PubMed: 11172029]
10. Chen Y, Cuda C, Morel L. Genetic determination of T cell help in loss of tolerance to nuclear antigens. J. Immunol. 2005; 174:7692–7702. [PubMed: 15944270]
11. Kumar KR, Li LN, Yan M, Bhaskarabhatla M, Mobley AB, Nguyen C, Mooney JM, Schatzle JD, Wakeland EK, Mohan C. Regulation of B cell tolerance by the lupus susceptibility gene Ly108. Science. 2006; 312:1665–1669. [PubMed: 16778059]
12. Chen Y, Perry D, Boackle SA, Sobel ES, Molina H, Croker BP, Morel L. Several genes contribute to the production of autoreactive B and T cells in the murine lupus susceptibility locus Sle1c. J. Immunol. 2005; 175:1080–1089. [PubMed: 16002709]
13. Wu H, Boackle SA, Hanvivadhanakul P, Ulgiati D, Grossman JM, Lee Y, Shen N, Abraham LJ, Mercer TR, Park E, Hebert LA, Rovin BH, Birmingham DJ, Chang DM, Chen CJ, McCurdy D, Badsha HM, Thong BY, Chng HH, Arnett FC, Wallace DJ, Yu CY, Hahn BH, Cantor RM, Tsao BP. Association of a common complement receptor 2 haplotype with increased risk of systemic lupus erythematosus. Proc. Natl. Acad. Sci. U.S.A. 2007; 104:3961–3966. [PubMed: 17360460]
14. Douglas KB, Windels DC, Zhao J, Gadeliya AV, Wu H, Kaufman KM, Harley JB, Merrill J, Kimberly RP, Alarcon GS, Brown EE, Edberg JC, Ramsey-Goldman R, Petri M, Reveille JD, Vila LM, Gaffney PM, James JA, Moser KL, arcon-Riquelme ME, Vyse TJ, Gilkeson GS, Jacob CO, Ziegler JT, Langefeld CD, Ulgiati D, Tsao BP, Boackle SA. Complement receptor 2 polymorphisms associated with systemic lupus erythematosus modulate alternative splicing. Genes Immun. 2009; 10:457–469. [PubMed: 19387458]

15. Wandstrat AE, Nguyen C, Limaye N, Chan AY, Subramanian S, Tian XH, Yim YS, Pertsemlidis A, Garner HR, Morel L, Wakeland EK. Association of extensive polymorphisms in the SLAM/CD2 gene cluster with murine lupus. Immunity. 2004; 21:769–780. [PubMed: 15589166]
16. Keszei M, Detre C, Rietdijk ST, Munoz P, Romero X, Berger SB, Calpe S, Liao G, Castro W, Julien A, Wu YY, Shin DM, Sancho J, Zubiaur M, Morse HC III, Morel L, Engel P, Wang N, Terhorst C. A novel isoform of the Ly108 gene ameliorates murine lupus. J. Exp. Med. 2011; 208:811–822. [PubMed: 21422172]
17. Brown DR, Calpe S, Keszei M, Wang N, McArdel S, Terhorst C, Sharpe AH. Cutting edge: An NK cell-independent role for Slamf4 in controlling humoral autoimmunity. J. Immunol. 2011; 187:21–25. [PubMed: 21622868]
18. Koh AE, Njoroge SW, Feliu M, Cook A, Selig MK, Latchman YE, Sharpe AH, Colvin RB, Paul E. The SLAM family member CD48 (Slamf2) protects lupus-prone mice from autoimmune nephritis. J. Autoimmun. 2011; 37:48–57. [PubMed: 21561736]
19. Cuda CM, Li S, Chen Y, Potula HSK, Xu Z, Butfiloski EJ, Chang LJ, Baker HV, Dozmorov I, Sobel ES, Morel L. Pre-B cell leukemia homeobox protein is associated with lupus susceptibility in mice and humans. J. Immunol. 2012; 188:604–614. [PubMed: 22180614]
20. Alaynick WA. Nuclear receptors, mitochondria and lipid metabolism. Mitochondrion. 2008; 8:329–337. [PubMed: 18375192]
21. Bettelli E, Carrier Y, Gao W, Korn T, Strom TB, Oukka M, Weiner HL, Kuchroo VK. Reciprocal developmental pathways for the generation of pathogenic effector TH17 and regulatory T cells. Nature. 2006; 441:235–238. [PubMed: 16648838]
22. Dozmorov I, Lefkovits I. Internal standard-based analysis of microarray data. Part 1: analysis of differential gene expressions. Nucleic Acids Research. 2009; 37:6323–6339. [PubMed: 19720734]
23. Dozmorov I, Centola M. An associative analysis of gene expression array data. Bioinformatics. 2003; 19:204–211. [PubMed: 12538240]
24. Xu Z, Vallurupalli A, Fuhrman C, Ostrov D, Morel L. An NZB-derived locus suppresses chronic graft versus host disease and autoantibody production through non-lymphoid bone-marrow derived cells. J. Immunol. 2011; 186:4130–4139. [PubMed: 21335485]
25. Stockinger B, Veldhoen M, Martin B. Th17 T cells: linking innate and adaptive immunity. Semin Immunol. 2007; 19:353–361. [PubMed: 18023589]
26. Dang E-V, Barbi J, Yang HY, Jinasena D, Yu H, Zheng Y, Bordman Z, Fu J, Kim Y, Yen HR, Luo W, Zeller K, Shimoda L, Topalian S-L, Semenza G-L, Dang C-V, Pardoll D-M, Pan F. Control of TH17/Treg Balance by Hypoxia-Inducible Factor 1. Cell. 2011; 146:772–784. [PubMed: 21871655]
27. Shi LZ, Wang R, Huang G, Vogel P, Neale G, Green DR, Chi H. HIF1à- dependent glycolytic pathway orchestrates a metabolic checkpoint for the differentiation of TH17 and Treg cells. J. Exp. Med. 2011; 208:1367–1376. [PubMed: 21708926]
28. McClymont SA, Putnam AL, Lee MR, Esensten JH, Liu W, Hulme MA, Hoffm++ller U, Baron U, Olek S, Bluestone JA, Brusko TM. Plasticity of human regulatory T cells in healthy subjects and patients with type 1 diabetes. J. Immunol. 2011; 186:3918–3926. [PubMed: 21368230]
29. Morris SC, Cheek RL, Cohen PL, Eisenberg RA. Autoantibodies in chronic graft versus host result from cognate T-B interactions. J. Exp. Med. 1990; 171:503–517. [PubMed: 2303783]
30. Giles BM, Tchepeleva SN, Kachinski JJ, Ruff K, Croker BP, Morel L, Boackle SA. Augmentation of NZB autoimmune phenotypes by the Sle1c murine lupus susceptibility interval. J. Immunol. 2007; 178:4667–4675. [PubMed: 17372026]
31. Alaynick WA, Way JM, Wilson SA, Benson WG, Pei L, Downes M, Yu R, Jonker JW, Holt JA, Rajpal DK, Li H, Stuart J, McPherson R, Remlinger KS, Chang CY, McDonnell DP, Evans RM, Billin AN. ERR g regulates cardiac, gastric, and renal potassium homeostasis. Mol. Endocrinol. 2010; 24:299–309. [PubMed: 19965931]
32. Lorke DE, Snsens U, Borgmeyer U, Hermans-Borgmeyer I. Differential expression of the estrogen receptor-related receptor g in the mouse brain. Mol. Brain Res. 2000; 77:277–280. [PubMed: 10837923]

33. Rangwala SM, Wang X, Calvo JA, Lindsley L, Zhang Y, Deyneko G, Beaulieu V, Gao J, Turner G, Markovits J. Estrogen-related receptor g is a key regulator of muscle mitochondrial activity and oxidative capacity. J. Biol. Chem. 2010; 285:22619–22629. [PubMed: 20418374]
34. Alaynick WA, Kondo RP, Xie W, He W, Dufour CR, Downes M, Jonker JW, Giles W, Naviaux RK, Giguere V, Evans RM. ERRgamma directs and maintains the transition to oxidative metabolism in the postnatal heart. Cell Metab. 2007; 6:13–24. [PubMed: 17618853]
35. Dufour CR, Wilson BJ, Huss JM, Kelly DP, Alaynick WA, Downes M, Evans RM, Blanchette M, Giguere V. Genome-wide orchestration of cardiac functions by the orphan nuclear receptors ERRalpha and gamma. Cell Metab. 2007; 5:345–356. [PubMed: 17488637]
36. Perl A, Gergely P Jr. Nagy G, Koncz A, Banki K. Mitochondrial hyperpolarization: a checkpoint of T-cell life, death and autoimmunity. Trends Immunol. 2004; 25:360–367. [PubMed: 15207503]
37. Cuda CM, Zeumer L, Sobel ES, Croker BP, Morel L. Murine lupus susceptibility locus Sle1a requires the expression of two sub-loci to induce inflammatory T cells. Genes Immun. 2010; 11:542–553. [PubMed: 20445563]
38. Pernis AB. Estrogen and CD4+ T cells. Curr. Opin. Rheumatol. 2007; 19:414–420. [PubMed: 17762604]
39. Mora JR, Iwata M, von Andrian UH. Vitamin effects on the immune system: vitamins A and D take centre stage. Nat. Rev. Immunol. 2008; 8:685–698. [PubMed: 19172691]
40. Glass CK, Saijo K. Nuclear receptor transrepression pathways that regulate inflammation in macrophages and T cells. Nat. Rev. Immunol. 2010; 10:365–376. [PubMed: 20414208]
41. Heard DJ, Norby PL, Holloway J, Vissing H. Human ERR g, a third member of the estrogen receptor-related receptor (ERR) subfamily of orphan nuclear receptors: tissue-specific isoforms are expressed during development and in the adult. Mol. Endocrinol. 2000; 14:382–392. [PubMed: 10707956]
42. Eichner LJ, Giguere V. Estrogen related receptors (ERRs): a new dawn in transcriptional control of mitochondrial gene networks. Mitochondrion. 2011; 11:544–552. [PubMed: 21497207]
43. Giguere V. Transcriptional control of energy homeostasis by the estrogen-related receptors. Endocr. Rev. 2008; 29:677–696. [PubMed: 18664618]
44. Takayanagi S, Tokunaga T, Liu X, Okada H, Matsushima A, Shimohigashi Y. Endocrine disruptor bisphenol A strongly binds to human estrogen-related receptor gamma (ERRgamma) with high constitutive activity. Toxicol. Lett. 2006; 167:95–105. [PubMed: 17049190]
45. Sawai C, Anderson K, Walser-Kuntz D. Effect of bisphenol A on murine immune function: modulation of interferon-gamma, IgG2a, and disease symptoms in NZB × NZW F1 mice. Environ. Health Perspect. 2003; 111:1883–1887. [PubMed: 14644661]
46. Michalek RD, Rathmell JC. The metabolic life and times of a T-cell. Immunol. Rev. 2010; 236:190–202. [PubMed: 20636818]
47. Vander Heiden MG, Cantley LC, Thompson CB. Understanding the Warburg effect: the metabolic requirements of cell proliferation. Science. 2009; 324:1029–1033. [PubMed: 19460998]
48. Eichner LJ, Perry MC, Dufour CR, Bertos N, Park M, St-Pierre J, Giguere V. miR-378(*) mediates metabolic shift in breast cancer cells via the PGC-1beta/ERRgamma transcriptional pathway. Cell Metab. 2010; 12:352–361. [PubMed: 20889127]
49. Jacobs SR, Herman CE, MacIver NJ, Wofford JA, Wieman HL, Hammen JJ, Rathmell JC. Glucose uptake is limiting in T cell activation and requires CD28-mediated Akt-dependent and independent pathways. J. Immunol. 2008; 180:4476–4486. [PubMed: 18354169]
50. Wang R, Dillon C-P, Shi L-Z, Milasta S, Carter R, Finkelstein D, McCormick L-L, Fitzgerald P, Chi H, Munger J, Green D-R. The transcription factor Myc controls metabolic reprogramming upon T lymphocyte activation. Immunity. 2011; 35:871–882. [PubMed: 22195744]
51. Hu W-H, Hausmann ON, Yan M-S, Walters WM, Wong PK, Bethea JR. Identification and characterization of a novel Nogo-inetracting mitochondrial protein (NIMP). J. Neurochem. 2002; 81:36–45. [PubMed: 12067236]
52. Giorgio V, Soriano ME, Basso E, Bisetto E, Lippe G, Forte MA, Bernardi P. Cyclophilin D in mitochondrial pathology. Biochem. Biophys. Act. 2010; 1797:1113–1118.

53. Deng W-J, Nie S, Dai J, Wu J-R, Zeng R. Proteome, phospoproteome, and hydroxyproteome of liver mitochondria in diabeteic rats at early pathogenic stages. Mol. Cell. Proteom. 2010; 9:100–116.

54. Michalek RD, Gerriets VA, Nichols AG, Inoue M, Kazmin D, Chang CY, Dwyer MA, Nelson ER, Pollizzi KN, Ilkayeva O, Giguere V, Zuercher WJ, Powell JD, Shinohara ML, McDonnell DP, Rathmell JC. Estrogen-related receptor-à is a metabolic regulator of effector T-cell activation and differentiation. Proc. Natl. Acad. Sci. U.S.A. 2011; 108:18348–18353. [PubMed: 22042850]

55. Crispin JC, Kyttaris VC, Terhorst C, Tsokos GC. T cells as therapeutic targets in SLE. Nat. Rev. Rheumatol. 2010; 6:317–325. [PubMed: 20458333]

56. Perl A, Gergely P Jr. Banki K. Mitochondrial dysfunction in T cells of patients with systemic lupus erythematosus. Int.Rev.Immunol. 2004; 23:293–313. [PubMed: 15204090]

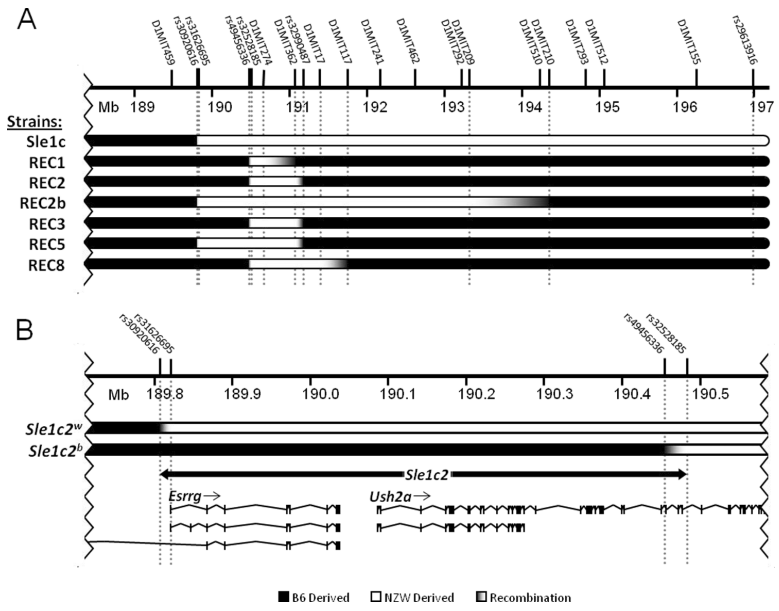

FIGURE 1.

Physical map of *Sle1c. A,* The *Sle1c* and its recombinant intervals (REC1 to REC8) are shown on the telomeric end of chromosome 1 with NZW-derived regions in white and B6-derived regions in black. All known polymorphic MIT microsatellite markers, as well as SNPs that define recombination intervals are depicted. *B, Sle1c2* is defined by the non-overlapping centrometric end of *Sle1c* that carries the NZW alleles in REC5 and REC2b (*Sle1c2*^{w}), and the B6 alleles in the other strains (*Sle1c2*^{b}). The SNPs defining the areas of recombination on both ends are shown, along with the exonintron structure of the two known protein coding genes located in *Sle1c2.* Scale is in Mb and all positions are current with Ensemble release 67 (www.ensembl.org/Mus_musculus/), which is based on NCBI m37.

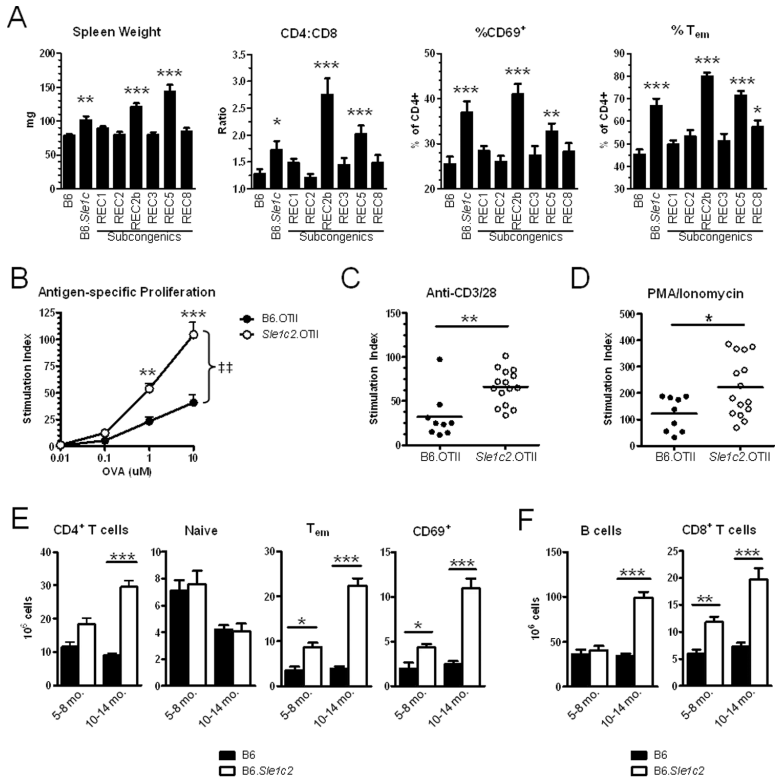

FIGURE 2.

Phenotypic mapping of *Sle1c2. A,* Comparison of spleen weights, CD4:CD8 ratios, CD69 expression and Tem percentages of $CD4^+$ T cells from spleens of 10–14 month old mice. Significance levels indicate ANOVA with Dunn's multiple comparison analysis to B6. Ag-specific (*B*), polyclonal (*C*), and PMA-induced (*D*) proliferation of $CD4^+$ T cells from 3–5 month old mice was measured by ^3H thymidine incorporation, and stimulation indexes were calculated relative to cultures with medium only. Both REC2b.OTII and REC5.OTII strains were used as *Sle1c2.*OTII. Two-way ANOVA (‡‡) was used to measure strain effect on Ag-specific proliferation with Bonferroni's post-test indicating significance at each concentration in *B.* Mann-Whitney was used in *C* and *t* test was used in *D.* Absolute numbers of splenic $CD4^+$ T cells (*E*) and of B and $CD8^+$ T cells (*F*) were compared between B6 and B6.*Sle1c2* at 5–8 and 10–14 month old cohorts. Naïve T cells were defined as $CD4^+$ $CD44^{lo}$ $CD62L^+$ and Tem cells were defined as $CD4^+$ $CD44^{hi}$ $CD62L^-$. Significance levels indicate Mann-Whitney comparisons to B6 mice of the same age group. * $P \leq 0.05$, ** $P \leq 0.01$, *** $P \leq 0.001$, ‡‡ $P \leq 0.001$.

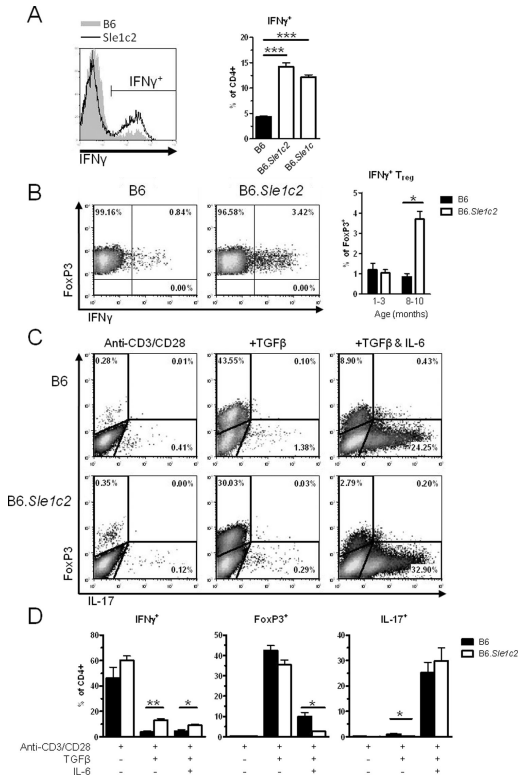

FIGURE 3.

Sle1c2 upregulates IFNγ expression. *A,* Representative histograms and quantification of *ex vivo* IFNγ intracellular staining in $CD4^+$ T cells were from the spleens of 2–3 month old mice. Significance levels indicate ANOVA with Dunn's multiple comparison analysis to B6. *B,* Representative plots and quantitation of $FoxP3^+$ $IFN\gamma^+$ double positive $CD4^+$ T cells after 3 d of culture with plate-bound anti-CD3/CD28 and TGFβ. Cells were collected from 1–3 and 8–10 month old mice. *C, D,* Representative plots (*C*) and quantification (*D*) of intracellular staining for IFNγ, FoxP3, and IL-17 in $CD4^+$ T cells from 8–10 month old mice after 3 d of TH0 (anti-CD3 and anti-CD28 only), Treg (stimulation plus TGFβ), and TH17 (stimulation plus TGFβ and IL-6) polarizing conditions. In B and D, *t* tests compare B6 to *Sle1c2* mice for each age or treatment group. : * $P \leq 0.05$, ** $P \leq 0.01$, *** $P \leq 0.001$.

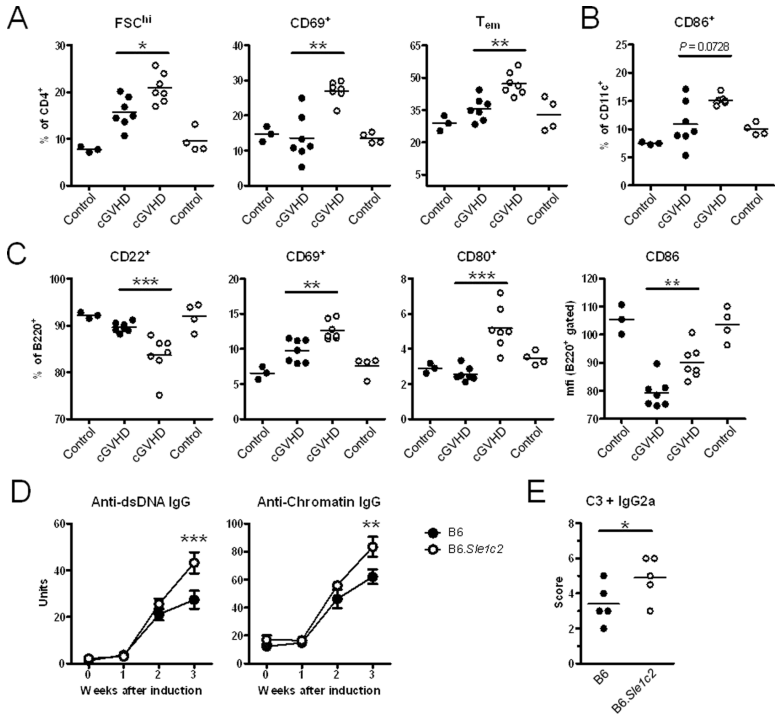

FIGURE 4.

Sle1c2 enhances induced lupus phenotypes in the cGVHD model. cGVHD was induced in B6 (filled circles) and B6.*Sle1c2* (open circles) and splenic compartments were compared by flow cytometry 3 weeks later. Age-matched non-induced mice are also shown as control. *A,* $CD4^+$ T cell activation was assessed by high forward scatter (indicative of blasting cells), CD69 expression and by expansion of T_{em} cells. *B,* Dendritic cell activation was indicated by B7–2 (CD86) expression. *C,* B cell activation was measured by CD22, CD69, B7–1 (CD80) and B7–2 expression. *D,* Glomerular IgG2a and C3 deposition was detected in frozen kidney sections. Sections were separately scored for each Ab and additive values (IgG2a score + C3 score) are shown. *E,* Weekly serum anti-chromatin and anti-dsDNA IgG were measured by ELISA. *A, B, C,* and *E* were compared by Mann-Whitney tests and *D* was compared by 2-way ANOVA with Bonferroni's post-test. * $P \leq 0.05$, ** $P \leq 0.01$, *** $P \leq 0.001$.

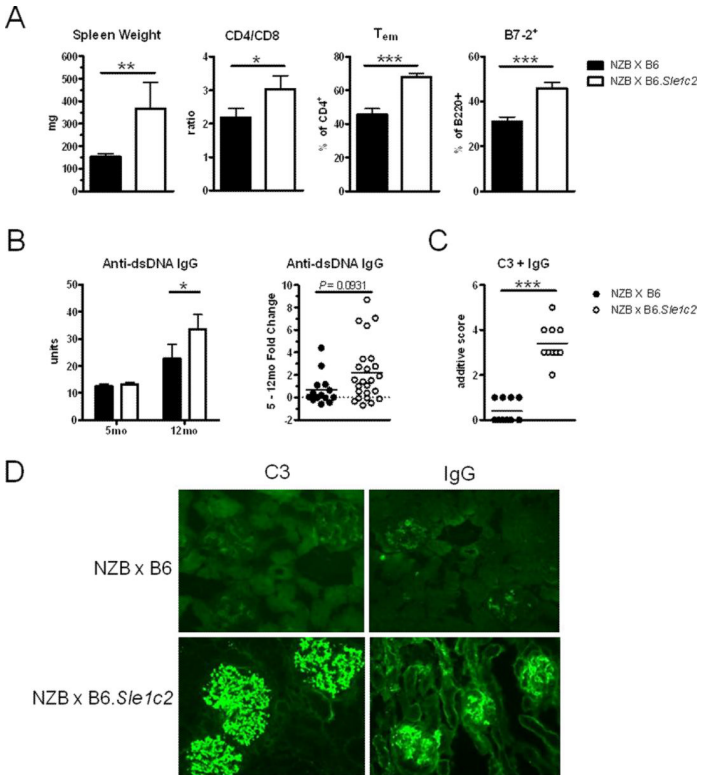

FIGURE 5.

Sle1c2 exacerbates spontaneous lupus phenotypes induced by the NZB genome. *A,* Spleen weight, CD4:CD8 ratios, percentage of $CD62L^{-}$ $CD44^{hi}$ $CD4^{+}$ and $B7\text{–}2^{+}$ $B220^{+}$ splenocytes in 12 month old (NZB × B6)F1 and (NZB × B6.*Sle1c2*)F1 mice (n=14 and 25, respectively). *B,* Serum anti-dsDNA IgG is shown as unit values at 5 and 12 months of age, and as relative individual increase between these two ages for each strain. *C* and *D,* Glomerular IgG and C3 deposition was detected in frozen kidney sections. Sections were separately scored for each Ab and additive values (IgG score + C3 score) are shown in *C.* Representative sections (X 100) are shown in *D.* Mann-Whitney tests: * $P \leq 0.05$, ** $P \leq 0.01$, *** $P \leq 0.001$.

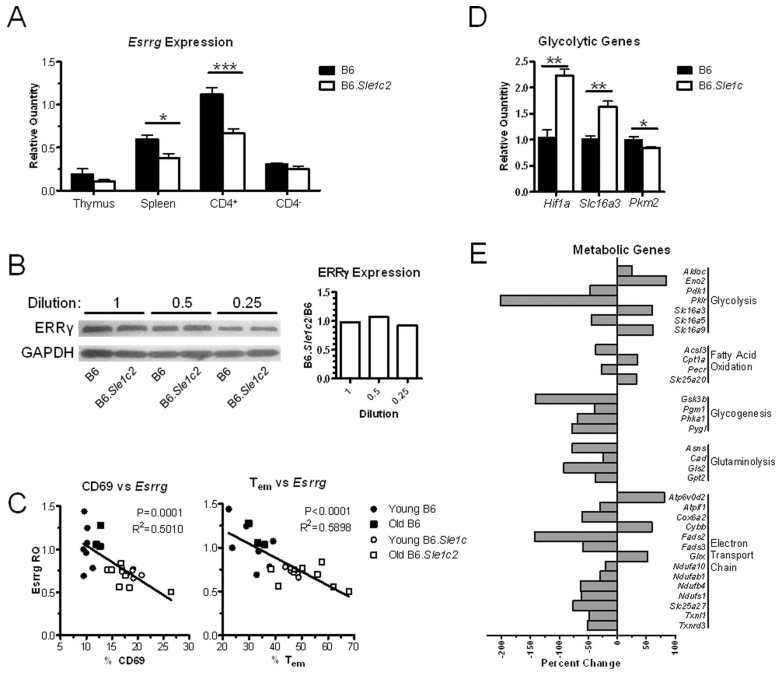

FIGURE 6.

Esrrg expression is decreased in *Sle1c2* CD4$^+$ T cells. *A,* qPCR comparing *Esrrg* expression in thymocytes, splenocytes, CD4$^+$ T cells, and CD4$^-$ fractions between B6 and B6.*Sle1c2* (8–10 month old, n=7 per strain). *t* tests were used to compare B6.*Sle1c2 Esrrg* expression to B6 for each cell population. *B,* ERRγ expression was analyzed in B6 and B6.*Sle1c2* CD4$^+$ T cells by semi-quantitative Western blotting, with cell lysates undiluted, diluted 1:2 (0.5) and 1:4 (0.25). The ERRγ protein abundance was normalized to the expression of GAPDH. The numbers in Y axis indicate the ratio of normalized ERRγ protein abundance in B6.*Sle1c2* CD4$^+$ cells to that in B6 CD4$^+$ cells. *C,* Correlation between *Esrrg* expression and CD69$^+$ and Tem percentages of splenic CD4$^+$ T cells. The young and old cohorts were 2–3 and 7–8 months old, respectively. The significance that slopes do not equal zero (P) and correlation coefficients for linear regressions (R^2) are shown. *D,* qPCR analysis of *Hif1a, Slc16a3,* and *Pkm2* expression in B6 and B6.*Sle1c2* CD4$^+$ splenocytes, compared with Mann-Whitney tests. *E,* Percent change in expression of genes in metabolic pathways from microarray analysis comparing B6.*Sle1c2* to B6 CD4$^+$ T cells. * $P \leq 0.05$, ** $P \leq 0.01$, *** $P \leq 0.001$.

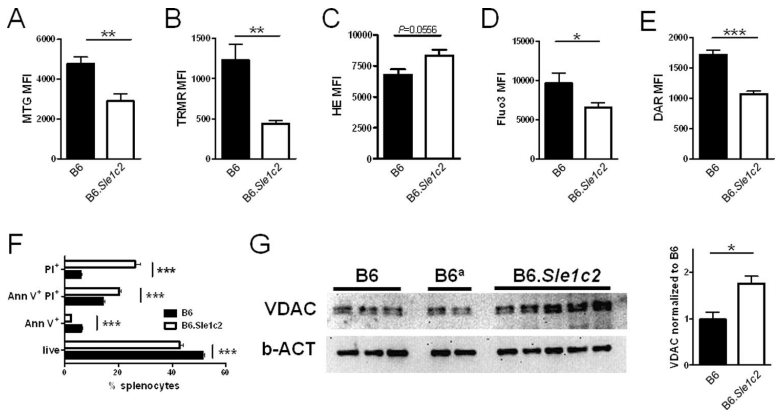

FIGURE 7.

Mitochondrial function is impaired in the CD4$^+$ T cells of B6.*Sle1c2* mice. *A–E,* Splenic CD3$^+$ CD4$^+$ T cells were assessed by flow cytometry for mitochondrial mass (*A*), mitochondrial membrane potential (*B*), oxidation (*C*), Ca (*D*) and NO (*E*) contents. The graphs show mean + SEM mean fluorescence intensity (MFI) normalized to B6 mean values. *F,* viability analysis of *ex-vivo* splenocytes based on Annexin V (Ann V) and PI staining. Live cells were Ann V$^-$ PI$^-$. *G,* VDAC expression in CD4$^+$ T cells analyzed by Western blot. β-actin expression is shown as a control. The graph on the right shows the densitometry analysis of the VDAC/ β-actin ratios normalized to one B6 sample. All data were collected from the same 2–3 months old mice. B6 and B6.Thy1^a (B6 ^{a}) values were pooled in the graphs under B6 and compared to B6.*Sle1c2* values with Mann-Whitney tests. * $P \leq 0.05$, ** $P \leq 0.01$, *** $P \leq 0.001$.

Table 1

Comparison of mitochondrial function in the major splenic cell subsets between B6.*Sle1c2* and B6 mice. MFI values were normalized to B6 means set at 1.0.

Cell type	MTG		TRMR		HE		DAR-4M		Fluo-3AM	
	B6	**Sle1c2**	**B6**	**Sle1c2**	**B6**	**Sle1c2**	**B6**	**Sle1c2**	**B6**	**Sle1c2**
$CD4^+$ T	1.04 + 0.09	0.65 + 0.80	0.96 + 0.18	0.31 + 0.03	0.98 + 0.08	1.16 + 0.07	1.03 + 0.07	0.65 + 0.03	0.96 + 0.12	0.62 + 0.06
CD8+ T	0.97 + 0.09	0.68+ 0.08	0.98 + 0.34	0.32 + 0.03	1.02 + 0.06	1.35 + 0.14	1.04+ 0.08	0.42 + 0.08	0.93 + 0.24	0.45 + 0.04
$CD19^+$	1.04 + 0.10	0.98 + 0.09	0.98 + 0.11	0.48 + 0.03	1.00 + 0.03	1.19 + 0.06	1.00 + 0.04	0.69 + 0.03	1.00 + 0.04	0.98 + 0.06
$CD11b^+$	0.98 + 0.20	0.97 + 0.13	1.43 + 0.92	0.35 + 0.03	0.98 + 0.05	1.18+ .02	0.99 + 0.04	0.54+ 0.06	1.00 + 0.28	0.79 + 0.04
$CD11c^+$	0.98 + 0.09	0.70 + 0.08	1.05 + 0.40	0.69 + 0.05	0.97 + 0.11	1.66 + 0.17	0.99 + 0.02	0.45 + 0.03	0.95+ 0.19	0.45 + 0.04

The values indicate mean ± SEM for 5 mice per strain.

Values were compared between the strains for each parameter.

Bold indicates $P < 0.05$,

underline indicates $P < 0.01$, and

double underline indicates $P < 0.001$.